In Silico Infrared and Raman Spectroscopy Under Pressure: The Case of CaSnO3 Perovskite.

J. Maul, A. Erba, I. M. G. Santos, J. R. Sambrano, R. Dovesi
In Silico Infrared and Raman Spectroscopy Under Pressure: The Case of CaSnO3 Perovskite.
THE JOURNAL OF CHEMICAL PHYSICS (2015) 142

In Silico Infrared and Raman Spectroscopy Under Pressure: The Case of $CaSnO_3$ Perovskite.

J. Maul,[1,2,3,a] A. Erba,[3] I. M. G. Santos,[1] J. R. Sambrano,[2] and R. Dovesi[3]

[1] *Laboratório de Combustíveis e Materiais, INCTMN-UFPB, Universidade Federal da Paraíba, CEP 58051-900, João Pessoa, PB, Brazil*

[2] *Grupo de Modelagem e Simulação Molecular, INCTMN-UNESP, Sao Paulo State University, CEP 17033-360, Bauru, SP, Brazil*

[3] *Dipartimento di Chimica, Università di Torino and NIS, Nanostructured Interfaces and Surfaces, Centre of Excellence, Via Giuria 5, 10125 Torino, Italy*

(Dated: 16 December 2014)

The $CaSnO_3$ perovskite is investigated under geochemical pressure, up to 25 GPa, by means of periodic *ab initio* calculations performed at B3LYP level with local Gaussian-type orbital basis sets. Structural, elastic and spectroscopic (phonon wave-numbers, infrared and Raman intensities) properties are fully characterized and discussed. The evolution of the Raman spectrum of $CaSnO_3$ under pressure is reported to remarkably agree with a recent experimental determination [*J. Chem. Phys.*, **135**, 224507 (2011)] as regards both wave-number shifts and intensity changes. All phonon modes are symmetry-labeled and bands assigned. The single-crystal total spectrum is symmetry-decomposed into the six directional spectra related to the components of the polarizability tensor. The infrared spectrum at increasing pressure is reported for the first time and its main features discussed. All calculations are performed using the CRYSTAL14 program taking advantage of the new implementation of analytical infrared and Raman intensities for crystalline materials.

Keywords: $CaSnO_3$ perovskite, pressure, Raman, CRYSTAL program

I. INTRODUCTION

Calcium stannate, $CaSnO_3$, is an alkaline earth perovskite of the ABO_3 family (where A sites host formally divalent cations, Ca^{2+}, and B sites are occupied by formally tetravalent cations, Sn^{4+}) that has received attention in recent years due to its peculiar physical and chemical properties which lead to many possible applications as capacitor component,[1,2] gas sensor,[3] high-capacity anode in Li-ion batteries,[4–6] catalyst,[7] and host for rare earth phosphors.[8–16]

At ambient conditions, calcium stannate is a $GdFeO_3$-type perovskite with an orthorhombic lattice characterized by the *Pbnm* space group and a structure which can be rationalized in terms of a framework of corner-sharing SnO_6 octahedra (see Figure 1). With respect to the ideal cubic structure, *Pm3m*, of many ABO_3 perovskites, SnO_6 octahedra are slightly tilted and distorted.[17,18] Structural and elastic properties of calcium stannate have been determined up to 8 GPa of pressure without any evidence of a phase transition,[19,20] which was suggested to occur at 12 GPa (from the $GdFeO_3$-type perovskite to the $CaIrO_3$-type post-perovskite structure) by a theoretical study, performed with the local-density-approximation (LDA) to the density-functional theory (DFT).[21] Given the geological interest of this mineral, being a structural analogue of the $MgSiO_3$ perovskite (one of the major constituents of the Earth lower mantle),[22] in recent years these findings further stimulated a great effort in the characterization of its properties under increasing pressures. X-ray diffraction experiments up to 26 GPa,[23] Raman scattering experiments up to 20 GPa,[23] elastic ultrasonic velocity measurements up to 18 GPa,[24] *in situ* synchrotron X-ray diffraction measurements up to 86 GPa and high temperatures[25] have been performed. No experimental evidence has been reported of such a phase transition to occur at predicted conditions of low temperature and pressure but rather at pressures above 40 GPa and temperatures above 2000 K.[25]

In recent years, many experimental studies have been performed in order to characterize the spectroscopic fingerprint of calcium stannate due to the short-range structural information (local distortions and symmetry) that can be inferred from it with respect to the long-range one that is commonly obtained from X-ray diffraction experiments. In this respect, a large variety of infrared (IR) and Raman scattering measurements have been reported.[7,14,23,25–33] Some of them measured Raman spectra at high temperatures[31] or pressures.[23] A recent theoretical study discussed the ambient pressure Raman spectrum just in terms of wave-numbers (intensities were not computed and, then, the full spectrum was not reproduced).[34]

Several features of the spectroscopic response of this mineral are still unknown, like the exact band assignment of all phonon modes, the single-crystal symmetry decomposition of the total Raman spectrum and the evolution under pressure of the IR spectrum. Taking advantage of the recent implementation in the CRYSTAL14 program[35,36] of an analytical scheme for the calculation of both IR and Raman wave-numbers and intensities,[37,38] in this paper we perform an *ab initio* study of structural, elastic and spectroscopic properties of $CaSnO_3$ under pressures up to 25 GPa. A computational setup

[a] Electronic mail: jeffdandrade@gmail.com

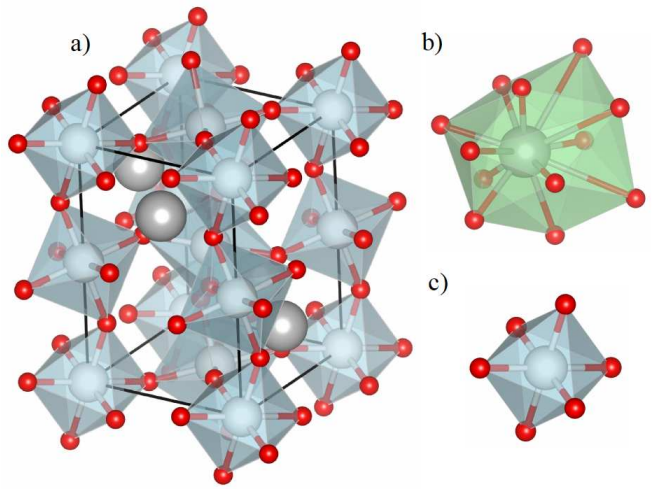

FIG. 1. (color online) a) structure of calcium stannate, $CaSnO_3$, in the *Pbnm* space group; b) CaO_{12} distorted cuboctahedron and c) SnO_6 octahedron.

consisting in the use of local Gaussian-type orbital basis sets and hybrid functional (B3LYP[39] in the present case) calculations is here adopted which has already been successfully applied to the study of structural, dielectric, elastic, piezoelectric and spectroscopic properties of other ABO_3 perovskites: $SrTiO_3$[40] and $BaTiO_3$.[41] The newly developed scheme for the simulation of Raman spectra, as combined with the above-mentioned computational setup, has recently been shown to provide reliable results for a wide range of materials.[36,42] Many automated algorithms, as implemented in the CRYSTAL14 program, for the theoretical determination of several properties of crystalline materials are here combined together in order to provide a reliable description of calcium stannate at high pressures: equation-of-state,[43,44] elastic tensor,[45,46] dielectric response,[47] phonon frequency[48] and IR and Raman intensity calculation.[37,38]

The structure of the paper is as follows: the used computational methods and details are given in Section II; results on structural, elastic and spectroscopic (IR and Raman) properties under pressure are described in Section III; conclusions are drawn in Section IV.

II. COMPUTATIONAL METHODOLOGY AND SETUP

The CRYSTAL14 program has been used for all the calculations reported in this study.[36] The B3LYP one-electron Hamiltonian is used, which contains a hybrid Hartree-Fock/Density-Functional exchange-correlation term. All-electron atom-centered Gaussian-type-function (GTF) basis sets are adopted. Ca, Sn and O atoms are described by a $8(s)6511(sp)21(d)$,[49] $9(s)763111(sp)631(d)$[50] and $6(s)2111(sp)1(d)$[51] contraction of primitive GTFs, respectively.

As implemented in the CRYSTAL program, infinite Coulomb and exchange sums are truncated according to five thresholds (here set to very tight values of 10, 10, 10, 10, 20).[35] A sub-lattice is defined with a shrinking factor of 6 for sampling the reciprocal space (corresponding to 64 **k**-points in the irreducible Brillouin zone). Numerical integration techniques are used for the evaluation of the DFT exchange-correlation contribution (see the `XXLGRID` keyword in the CRYSTAL User's Manual). The convergence of the self-consistent-field (SCF) step of the calculation is governed by a threshold on energy of 10^{-10} hartree for geometry optimizations and 10^{-11} hartree for phonon frequency and equation-of-state calculations.

Equilibrium and strained configurations are optimized by use of analytical energy gradients calculated with respect to both atomic coordinates and unit-cell parameters or atomic coordinates only, respectively.[52,53] A quasi-Newtonian technique is used, combined with the Broyden-Fletcher-Goldfarb-Shanno (BFGS) algorithm for Hessian updating.[54–57] Convergence is checked on both gradient components and nuclear displacements; the corresponding tolerances on their root mean square are chosen to be more severe than the default values for simple optimizations: 0.0001 a.u. and 0.0004 a.u., respectively.

A. Equation of State

A commonly-adopted approach in solid state quantum chemistry for computing the pressure-volume relation of a crystalline material is via so-called Equations of State (EOS). "Cold" EOSs are energy-volume (or pressure-volume) analytical relations which describe the behavior of a solid under compression and expansion, at $T = 0$ K (that is the case of standard *ab initio* simulations) and are commonly used in solid state physics and geophysics.[58,59] Energy-volume data are numerically fitted to the analytical $E(V)$ functional form of the EOS. From $P = -\partial E/\partial V$, the P-V connection is established. The explicit dependence of the bulk modulus on volume (or pressure) is then given by $K(V) = V\partial^2 E/\partial V^2$.

Four EOSs are currently implemented in the CRYSTAL14 program (the full EOS calculation is activated by a single keyword):[43] the third-order Murnaghan (M),[60] the third-order Birch-Murnaghan (BM),[61,62] the logarithmic Poirier-Tarantola (PT)[63] and the exponential Vinet (Vin).[64] The energy of the system has been minimized at 21 different volumes in a range from -15% of compression to +15% of expansion with respect to the equilibrium volume V_0.

B. Elastic Tensor

The accuracy of the equation-of-state approach discussed above can be checked by comparing the value of the equilibrium bulk modulus, K^{EOS}, with the one that can be obtained from the knowledge of the elastic tensor

of the system, $K^{\rm elast}$. If any finite pre-stress is absent, second-order elastic constants are simply defined as second energy density derivatives with respect to pairs of infinitesimal Eulerian strains:

$$C_{ijkl} = \frac{1}{V_0}\left(\frac{\partial^2 E}{\partial\epsilon_{ij}\partial\epsilon_{kl}}\right)_{\epsilon=0} . \quad (1)$$

An automated scheme for the calculation of the elastic tensor, **C**, (and of its inverse, the compliance tensor $\mathbf{S} = \mathbf{C}^{-1}$) has been implemented in the CRYSTAL program,[45] that has been generalized also to low-dimensional, 1D and 2D, systems.[65] A two-index representation of the elastic tensor is obtained ($C_{ijkl} \rightarrow C_{vu}$) by exploiting Voigt's notation, according to which $v, u = 1, \ldots, 6$ ($1 = xx$, $2 = yy$, $3 = zz$, $4 = yz$, $5 = xz$, $6 = xy$).[66] This symmetric tensor exhibits, in general, 21 independent elements that reduce to 9 (*i.e.* C_{11}, C_{12}, C_{13}, C_{22}, C_{23}, C_{33}, C_{44}, C_{55} and C_{66}) for crystals with orthorhombic symmetry, as in the case of calcium stannate. A number of elastic properties (such as bulk modulus, $K^{\rm elast}$, shear modulus, $G^{\rm elast}$,Young modulus, Poisson's ratio, etc.) can be deduced from the elastic constants.[66,67] For the elastic constant calculation, two strained configurations are considered for each independent strain, with a dimensionless strain amplitude of 0.015.

C. Phonon Frequencies and Raman Intensities

Harmonic phonon frequencies (*i.e.* wave-numbers), ω_p, at the Γ point (*i.e.* at the center of the first Brillouin zone in reciprocal space) are obtained from the diagonalization of the mass-weighted Hessian matrix of the second energy derivatives with respect to atomic displacements u:[48,68]

$$W^{\Gamma}_{ai,bj} = \frac{H^{\mathbf{0}}_{ai,bj}}{\sqrt{M_a M_b}} \quad \text{with} \quad H^{\mathbf{0}}_{ai,bj} = \left(\frac{\partial^2 E}{\partial u^{\mathbf{0}}_{ai}\partial u^{\mathbf{0}}_{bj}}\right) , \quad (2)$$

where atoms a and b (with atomic masses M_a and M_b) in the reference cell, **0**, are displaced along the i-th and j-th Cartesian directions, respectively. Default tolerances are used for this task.[35]

The Raman intensity of the Stokes line of a phonon mode Q_p, characterized by a frequency ω_p, active due to the $\alpha_{ii'}$ component of the polarizability tensor α, is given by:

$$I^p_{ii'} \propto \frac{(\omega_L - \omega_p)^4}{30\omega_p\left[1 - \exp\left(-\frac{\hbar\omega_p}{K_B T}\right)\right]}\left(\frac{\partial\alpha_{ii'}}{\partial Q_p}\right)^2 , \quad (3)$$

where the pre-factor depends on laser frequency ω_L and temperature T:[69] in the present study, $T = 298.15$ K and ω_L corresponds to a wavelength of 514 nm which are the same parameters used in the experiment by Kung *et al.*[23] we compare with. The relative Raman intensities of the peaks are computed analytically by exploiting a scheme, recently implemented in the CRYSTAL14 program.[37,38] Both schemes are based on the solution of first- and second-order Coupled-Perturbed-Hartree-Fock/Kohn-Sham (CPHF/KS) equations.[47] From equation (3), we can clearly see that six symmetry-independent directional Raman spectra can be computed for a single-crystal which correspond to the six independent components of the polarizability tensor.

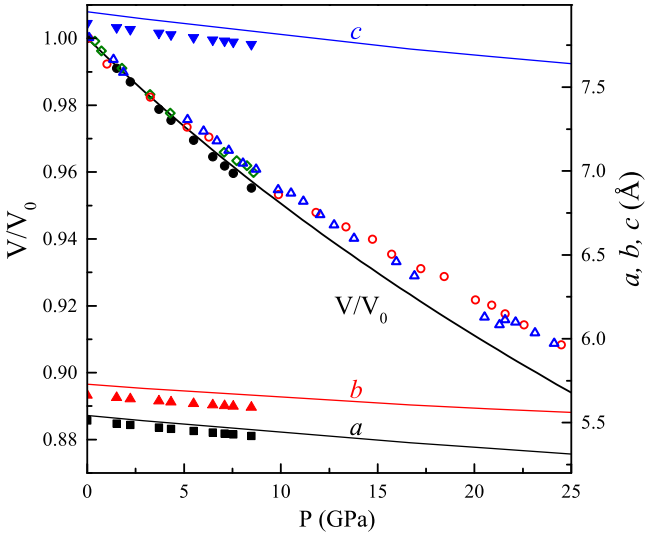

FIG. 2. (color online) Evolution under pressure of (right scale) the three lattice parameters a, b and c and (left scale) the V/V_0 ratio for the $CaSnO_3$ perovskite in the *Pbnm* space group. Continuous lines represent computed values. Experimental data by Kung *et al.*[19] from a single-crystal X-ray diffraction experiment are reported as full symbols (squares for a, triangles for b, inverse triangles for c and circles for V/V_0). For V/V_0, other experimental data by Kung *et al.*[23] referring to a polycrystalline sample are reported as empty symbols (different symbols refer to different runs).

III. RESULTS AND DISCUSSION

A. Structural and Elastic Properties

Before discussing the effect of pressure on spectroscopic properties, we report computed structural properties up to 26 GPa of pressure and we compare them with available experimental data and previously computed data. We have adopted an EOS approach (see Section II A for practical details) for obtaining the pressure-volume relation of $CaSnO_3$.

In Figure 2, we report the V/V_0 ratio and the absolute values of the three lattice parameters, a, b and c, of calcium stannate, as a function of pressure. Our computed values, reported as continuous lines, are compared with accurate single-crystal X-ray diffraction values,[19] given as full symbols. The figure clearly shows that our B3LYP calculations slightly overestimate the lengths of the three lattice parameters (by 0.5%, 1.2% and 0.9% at

TABLE I. Equilibrium bulk modulus, K_0, its pressure derivative, K_0' and the equilibrium volume V_0 of $CaSnO_3$ as computed with an EOS approach in the present study (see text for details) and compared with experimental (at room temperature) and previous theoretical data.

	K_0 (GPa)	K_0'	V_0 (Å^3)
Exp.[24]	166	5.4	-
Exp.[19]	163	5.6	246.1
This study (B3LYP)	179	4.0 - 4.1	252.5
Cherrad *et al.*[70] (LDA)	182	-	235.5
Yangthaisong[34] (LDA)	200	-	232.6
Yangthaisong[34] (GGA)	182	-	241.7
Tsuchiya and Tsuchiya[21] (LDA)	172	3.5	243.7

zero pressure for a, b and c, respectively). Inclusion of zero-point motion (ZPM) and other thermal effects (here neglected) would further increase computed lattice parameters. However, their pressure dependence is found to be in remarkable agreement with the experimental counterpart. Overall, this can be seen from the good agreement of the computed V/V_0 ratio with data by Kung *et al.*[19] Other experimental data are reported in the figure for the V/V_0 ratio obtained from polycrystalline X-ray diffraction experiments[23] (empty symbols) which are found to significantly deviate from both the other experimental determinations and our computed values.

As introduced in Section II A, four different expressions of EOSs have been used to fit energy-volume data. Different EOSs provide very similar values: the bulk modulus is predicted to be 179 GPa, its pressure derivative between 4.0 and 4.1 and the equilibrium volume to be 252.5 Å. In Table I, we report these computed parameters as compared with available experimental data and previous theoretical results. As expected, experimental determinations of the bulk modulus are lower (166 GPa according to Schneider *et al.*[24] and 163 according to Kung *et al.*[19]). This is partially due to the fact that our computed values refer to zero temperature and, moreover, neglect ZPM effects which are known to reduce computed bulk moduli and increase computed equilibrium volumes.[71] By explicitly including the ZPM effect, the computed bulk modulus becomes 176.6 GPa at zero temperature and further decreases to 173 GPa at 300 K, reducing the difference with respect to the experiment to about 5%. Surprisingly enough, given the satisfactory description of the V/V_0 dependence on pressure, our computed values for K_0' are significantly lower than available experimental determinations (in the range of 5.4-5.6). Results from previous *ab initio* calculations show a large underestimation of the equilibrium volume (more so at LDA level than at GGA, generalized-gradient approximation, level) and a corresponding overestimation of the bulk modulus (in the range 182-200 GPa), apart from the first LDA study by Tsuchiya and Tsuchiya[21] that provides values in closer agreement with the experiment.

TABLE II. Equilibrium elastic properties of $CaSnO_3$. Single-crystal elastic constants, C_{vu} (in GPa), and VRH average isotropic polycrystalline bulk modulus, $\overline{K}$ (in GPa), shear modulus, $\overline{G}$ (in GPa), Young modulus, $\overline{E}$ (in GPa), Poisson ratio, $\overline{\sigma}$ (dimensionless), longitudinal and transverse seismic wave velocities, $\overline{v}_p$ and $\overline{v}_s$ (in km/s). Experimental data refer to room temperature.

	C_{11}	C_{22}	C_{33}	C_{44}	C_{55}	C_{66}	C_{12}	C_{13}	C_{23}	$\overline{K}$	$\overline{G}$	$\overline{E}$	$\overline{\sigma}$	$\overline{v}_p$	$\overline{v}_s$
Exp.[24]	-	-	-	-	-	-	-	-	-	166	88	-	-	7.28	4.02
Exp.[19]	-	-	-	-	-	-	-	-	-	163	89	-	-	-	-
This study (B3LYP)	325	304	289	85	98	102	110	130	109	179	95	242	0.28	7.48	4.16
Cherrad *et al.*[70] (LDA)	285	335	318	104	85	107	138	107	107	182	-	-	-	-	-
Yangthaisong[34] (LDA)	340	348	347	133	117	111	131	132	121	182	111	-	-	-	-
Yangthaisong[34] (GGA)	325	323	318	129	118	100	108	116	111	200	115	-	-	-	-

In order to verify the numerical accuracy of our EOS determination of the bulk modulus, $K^{\rm EOS}$, of calcium stannate, we have computed the full fourth-order elastic tensor of the system (following the procedure sketched in Section II B), from which an independent estimate, $K^{\rm elast}$, can be obtained of the bulk modulus. From the

knowledge of the elastic tensor, a variety of elastic properties of the system can be deduced. The Voigt-Reuss-Hill (VRH) averaging scheme provides expressions for computing the average bulk and shear moduli ($\overline{K}$ and $\overline{G}$, respectively) for an isotropic polycrystalline aggregate from the elastic and compliance constants.[72] From these properties, Young's modulus, E, and Poisson's ratio, σ, can be defined as well:

$$E = \frac{9\overline{K}\overline{G}}{3\overline{K}+\overline{G}} \quad \text{and} \quad \sigma = \frac{3\overline{K}-2\overline{G}}{2(3\overline{K}+\overline{G})} \,. \tag{4}$$

Average values of transverse (shear) and longitudinal seismic wave velocities can also be computed from $\overline{K}$, $\overline{G}$ and the density ρ of the crystal as:[73]

$$\overline{v}_s = \sqrt{\frac{\overline{G}}{\rho}} \quad \text{and} \quad \overline{v}_p = \sqrt{\frac{\overline{K}+4/3\overline{G}}{\rho}} \,. \tag{5}$$

All these elastic properties are reported in Table II as computed in the present study and as compared with available experimental and previous theoretical values. We notice that the value of the bulk modulus that we get from the elastic tensor evaluation, 179 GPa, perfectly agrees with those found with different EOSs, 179 GPa, thus confirming the excellent numerical accuracy of all the used algorithms. As already noticed for the bulk modulus, also our computed shear modulus, $\overline{G}$, is slightly overestimated (95 GPa with respect to experimental values of 88-89 GPa). Schneider *et al.*[24], in their ultrasonic velocity study, have reported experimental values of $\overline{v}_p$ and $\overline{v}_s$. Our computed values are slightly overestimated: 7.48 km/s with respect to 7.28 km/s for $\overline{v}_p$ and 4.16 km/s with respect to 4.02 km/s for $\overline{v}_s$. Given relations (5), this overestimation of the seismic wave velocities can be understood in terms of our slight overestimation of the elastic moduli and of the equilibrium volume (and, then, of the slight underestimation of the density ρ of the system). To the best of our knowledge, there are no experimental single-crystal elastic constants for $CaSnO_3$ to compare with. In this respect, in Table II, we just report previous theoretical determinations. All studies but the GGA one by Yangthaisong[34] agree on the relative order of different subsets of elastic constants: diagonal constants (C_{11}, C_{22} and C_{33}) are larger than off-diagonal ones (C_{12}, C_{13} and C_{23}) which are in turn larger than shear ones (C_{44}, C_{55} and C_{66}).

Let us now briefly illustrate the dependence on pressure of the main interatomic distances in *Pbnm* calcium stannate. The two main structural sub-units in $CaSnO_3$ are the SnO_6 octahedra and the CaO_{12} distorted cuboctahedra (see Figure 1 for a graphical representation of the two sub-units). The Ca site, that in the perfect cubic perovskite structure would be cuboctahedral, in the *Pbnm* space group appears to be rather distorted so that it can be considered either as a CaO_{12} polyhedron or as a CaO_8 polyhedron. CaO_{12} (or CaO_8) sub-units have been found to be more compressible than SnO_6 ones.[20] In Figure 3 we report symmetry-independent interatomic

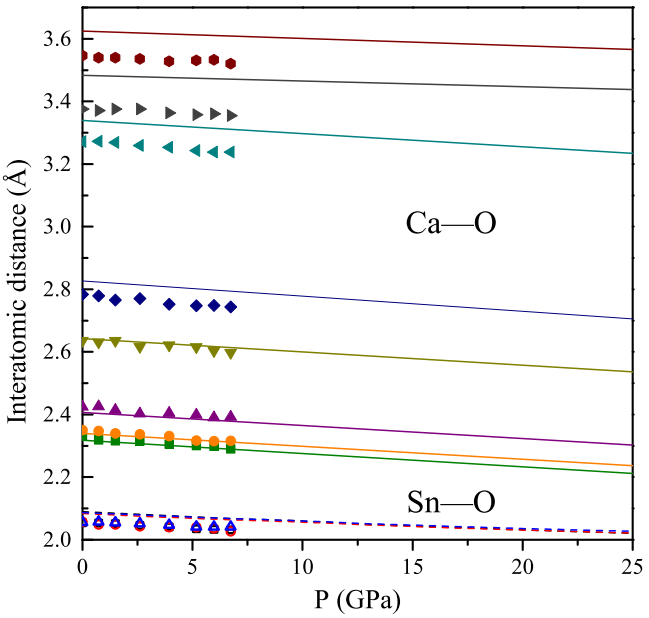

FIG. 3. (color online) Some interatomic distances in *Pbnm* calcium stannate as a function of pressure. Dashed and continuous lines represent computed Sn−O distances of the SnO_6 octahedral sub-units and Ca−O distances of the CaO_{12} sub-units, respectively. Experimental data, up to 7 GPa, from Zhao *et al.*[20] are reported as symbols (full symbols refer to the 8 symmetry-independent Ca−O distances and open symbols to the 2 Sn−O ones).

distances of both sites of calcium stannate, as a function of pressure. Lines are used to represent computed data, which are compared with available experimental data from Zhao *et al.*[20], up to 7 GPa. From the analysis of the three symmetry-independent Sn−O distances of the SnO_6 sub-unit (almost undistinguishable at this scale) and of the five smallest symmetry-independent Ca−O distances of the CaO_8 sub-unit, we can clearly see that: i) all distances are slightly overestimated, as expected from the overall overestimation of the volume; ii) the slope of each distance with respect to pressure is in remarkable agreement with experimental data; iii) the compressibility of Ca−O bonds is larger than Sn−O ones. This can be easily understood in terms of their degree of covalency; according to a Mulliken partition of the electronic charge density, the net charges are +1.6 (Ca), +1.7 (Sn) and -1.1 (O) $|e|$ and the bond overlap population is about 0.03 and 0.15 $|e|$ for Ca−O and Sn−O bonds, respectively, confirming that the Ca−O bonds are essentially ionic, whereas Sn−O bonds have a strong covalent character. The three largest Ca−O interatomic distances (> 3.2 Å) are proper of the CaO_{12} polyhedron (not of the CaO_8 one), are largely overestimated but, as discussed by Zhao *et al.*,[20] are not directly related to the compressibility of the structure but rather to the octahedral tilting of the framework.

As a final remark, we also note that the current description of the electronic structure of calcium stannate

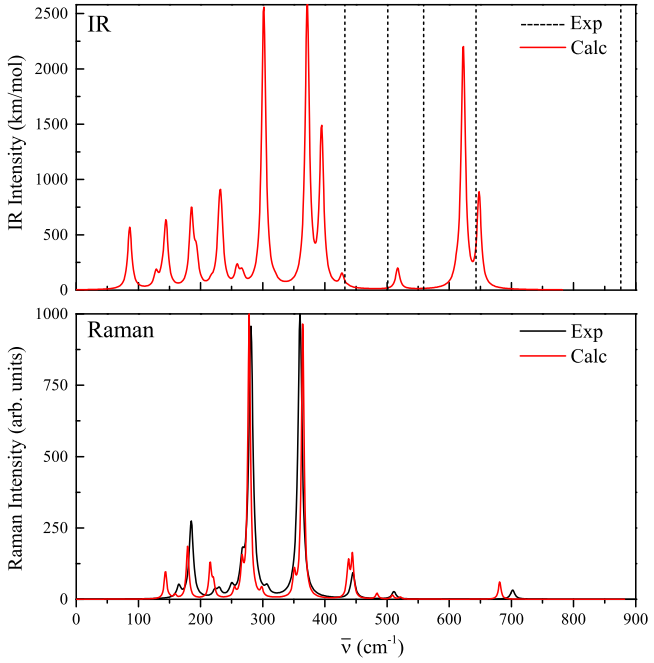

FIG. 4. (color online) Computed IR and Raman spectra of calcium stannate at zero pressure (red lines). In the upper panel, experimental wave-numbers as determined from IR measurements[33] are reported as vertical dashed lines. In the lower panel, the experimental Raman spectrum measured by Kung *et al.*[23] is reported (black line). Computed spectra are redshifted by 18 cm^{-1}.

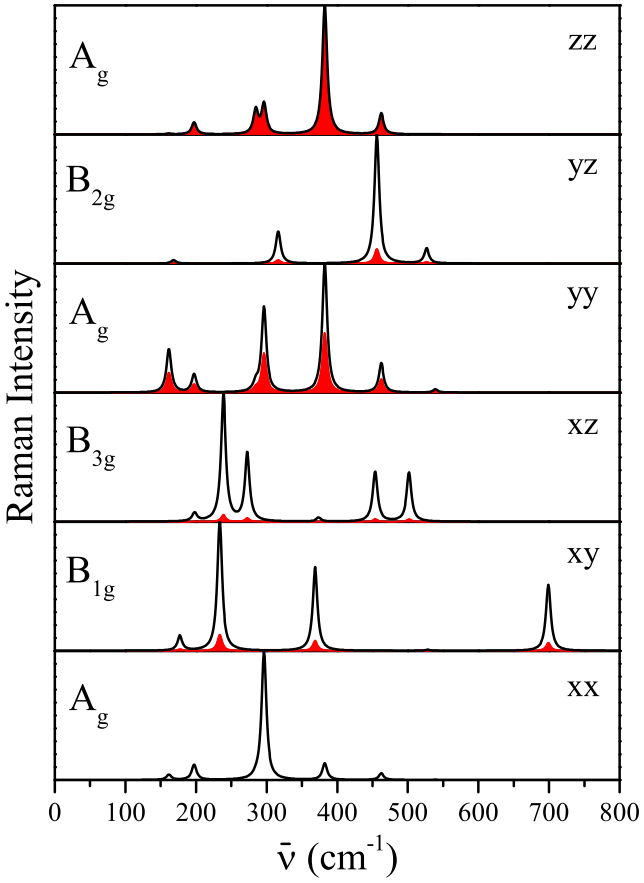

FIG. 5. (color online) Computed single-crystal directional Raman spectra of the $CaSnO_3$ perovskite at 514 nm wavelength and 298.15 K. See text for the definition of the reported curves.

closely resembles the experimental one, with a computed band gap of 4.87 eV with respect to experimental values of 4.40 eV[74] and 4.44 eV.[7] In this respect, as expected, the present computational setup, based on hybrid B3LYP calculations, is found to significantly improve over previous *ab initio* theoretical descriptions of the electronic structure of $CaSnO_3$, at LDA and GGA level, which reported largely underestimated band gap values, in the range 1.95-3.10 eV.[34,70,75]

B. Spectroscopic Properties

In this section, spectroscopic properties of $CaSnO_3$ (IR and Raman spectra) will be reported as computed *ab initio* as a function of pressure. The unit cell of *Pbnm* calcium stannate contains 20 atoms; the 57 corresponding vibration frequencies (excluding the three translations) are computed following the procedure described in Section II C by diagonalizing the dynamical matrix of equation (2). The symmetry properties of all phonon modes can be described in terms of the following partition of the reducible representation built on the basis of the Cartesian coordinates of the atoms in the cell:

$$\Gamma_{total} = 7A_g \oplus 5B_{1g} \oplus 5B_{2g} \oplus 7B_{3g} \oplus 8A_u \oplus 9B_{1u} \oplus 9B_{2u} \oplus 7B_{3u} \; . \quad (6)$$

All phonon modes are non degenerate. Among them, 25 are IR active (B_{1u}, B_{2u} and B_{3u}) and 24 Raman active (A_g, B_{1g}, B_{2g} and B_{3g}). Out of the 24 active Raman modes, previous Raman scattering experiments on polycrystalline samples could detect just 9 to 12 modes.[7,23,29,30] The experimental characterization of the IR spectrum is much poorer: only 5 peaks, out of 25, were reported,[33] among which only 3 find a correspondence with current computed ones. Present theoretical calculations obviously provide all of them. Graphical animations of all the vibration modes are available to the readers, which allow for a detailed assignment.[76] IR and Raman intensities have been computed analytically, using a CPHF/KS approach, as briefly recalled in Section II C. As regards the pressure dependence of the spectroscopic response, from an experimental point of view, an accurate study of the Raman spectrum has been reported up to 20 GPa,[23] whereas, to the best of our knowledge, no IR data are available.

Before discussing the evolution under pressure of the spectra, let us discuss the zero pressure ones and compare them with available experimental measurements. In Figure 4, we report the computed zero pressure IR and

TABLE III. Zero pressure wave-numbers $\overline{\nu}_0$ (in cm^{-1}) and slope d$\overline{\nu}$/dP (in cm^{-1}/GPa) of their pressure dependence for selected modes (*i.e.* those experimentally available) of $CaSnO_3$. Experimental data are from Kung *et al.*[23]

Mode	$\overline{\nu}_0$		d$\overline{\nu}$/dP	
	Exp.	Calc.	Exp.	Calc.
#1 A_g	163	161	2.28	2.13
#2 A_g	183	197	1.29	1.07
#3 B_{1g}	227	233	1.65	1.50
#4 B_{3g}	245	272	2.86	2.24
#5 A_g	264	284	2.67	1.89
#6 A_g	278	296	1.94	1.74
#7 A_g	358	382	4.35	3.82
#8 A_g	443	462	3.06	2.84

Raman spectra of calcium stannate (red curves).

As regards the IR part, a recent study by Zheng *et al.*[33] reported an IR transmittance spectrum of $CaSnO_3$ in the range 400-2000 cm^{-1}. As anticipated, only five peaks were reported (whose position in the spectrum is represented by vertical dashed lines in the upper panel of Figure 4) and tentatively assigned to stretching modes of Sn−O bonds and librations of the SnO_6 octahedra. Out of these 5 peaks, only 3 are found to somehow correspond to our theoretical description: the ones at 432 cm^{-1}, 501 cm^{-1} and 643 cm^{-1}. In particular, the last one has been reported to be the most intense and, indeed, is close to the most intense peak in the simulated spectrum in that region. The other two experimentally reported peaks (at 559 cm^{-1} and 876 cm^{-1}) do not find any correspondence in our computed spectrum and are likely to be considered as spurious signals in the recorded spectrum. Most of the IR fingerprint of $CaSnO_3$, however, is found below 400 cm^{-1} (see upper panel in the figure), a region that was not explored by Zheng *et al.*[33] Overall, the experimental characterization of the IR spectrum is rather poor; a much richer description to compare with is available as regards the Raman spectrum.

In the lower panel of Figure 4, our computed total Raman spectrum (red curve) is compared with the accurate experimental determination by Kung *et al.*[23] from their Raman scattering experiment on a polycrystalline sample (black curve). After having redshifted our computed spectrum by 18 cm^{-1}, the agreement between the two can be considered rather satisfactory, as regards both relative peak location and intensity. The spectrum is dominated by two high-intensity peaks at about 270 cm^{-1} and 360 cm^{-1} with very similar intensities. The information content of our single-crystal theoretical simulation is much larger than that of a polycrystalline measurement. The total Raman spectrum of calcium stannate can, indeed, be decomposed into six directional components (each one corresponding to an independent element of the polarizability tensor, see equation 3) with contributions from specific phonon modes of given symmetry (irreducible representations of the group). In Figure 5, we report such directional Raman spectra; in all panels, but the bottom one, red spectra report the intensity relative to the xx component (bottom panel). The black line represents spectra where the highest peaks of all panels are normalized to the same value to highlight features of low-intensity components. Diagonal xx, yy and zz components arise from A_g phonon modes whereas off-diagonal components, xy, xz and yz, from B_{1g}, B_{3g} and B_{2g} phonon modes, respectively. The diagonal components are very intense, xx and zz more so than yy and are essentially the responsible for the two high-intensity peaks mentioned above. The off-diagonal components show a low intensity, particularly so for the xz one. These theoretical predictions could be verified by highly accurate single-crystal directional Raman scattering experiments, as already reported for the $CaTiO_3$ perovskite.[29]

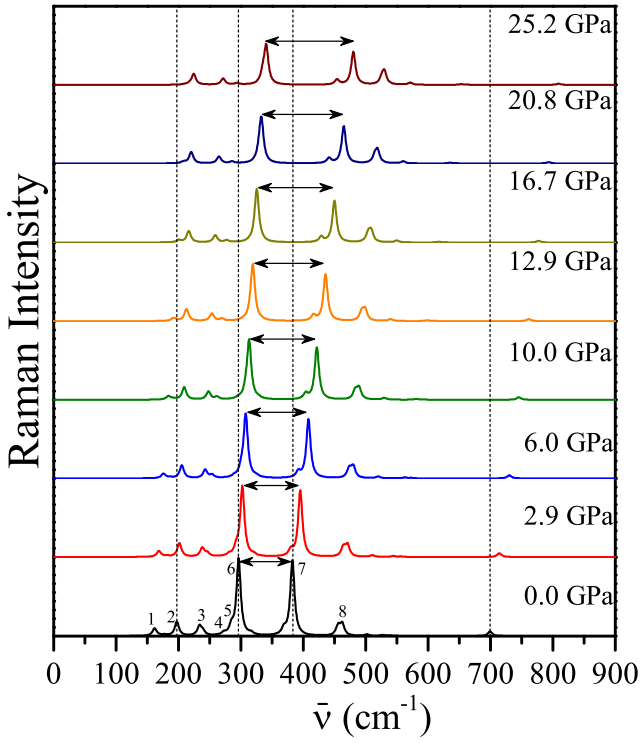

FIG. 6. (color online) Evolution under pressure, up to 25 GPa, of the computed Raman spectrum of $CaSnO_3$. Intensities at all pressures are relative to the zero-pressure ones. The width of the horizontal arrows represents the experimental separation between the two most intense peaks in the spectrum, as obtained by fitting measured data by Kung *et al.*[23] The vertical dashed lines are just an eye-guide. In the zero pressure spectrum, selected peaks are labeled according to Table III.

We now analyze the effect of pressure on the spectroscopic response of calcium stannate. In their recent work, Kung *et al.*[23] have measured the polycrystalline Raman spectrum of $CaSnO_3$ under pressures up to 20 GPa. In the zero pressure spectrum, they could identify

10 peaks which, however, reduced to 8 in the diamond anvil cell experiments at high pressures, thus restricting the explored range to 0-550 cm^{-1}. For these 8 peaks, they could determine the slope $d\overline{\nu}/dP$ (the pressure dependence of the corresponding wave-numbers). These data are reported in Table III and compared with our computed values. Experimental and computed wave-numbers at zero pressure, $\overline{\nu}_0$, are also reported, along with our symmetry assignment. From the analysis of the table we can deduce that: i) apart from the very first peak, as already mentioned before, our computed wave-numbers are blue-shifted by about 15-20 cm^{-1} with respect to experimental ones; ii) the computed pressure dependence of wave-numbers is found to remarkably match the experimental one, in particular as regards the relative slopes among those modes. If we sort these 8 modes in terms of decreasing slope, indeed, we get #7≫#8>#4>#5>#1>#6>#3>#2 according to the experiment and #7≫#8>#4>#1>#5>#6>#3>#2 from our computed data.

In Figure 6, we report the computed overall Raman spectrum of $CaSnO_3$ as a function of pressure. All spectra are relative to the zero pressure one. At each pressure, the horizontal arrow represents the experimental separation between the two most intense peaks of the spectrum, as obtained by fitting measured data by Kung *et al.*[23] Vertical dashed lines are eye-guides aligned to selected zero pressure peaks to highlight peak shifts under pressure. From inspection of the figure, some observations can be deduced. All peaks in the spectrum are blue-shifted by pressure but with quite different speeds. Let us consider, for instance, the two most intense peaks of the spectrum (modes #6 and #7 in Table III); it is clearly seen how the second one shifts more than the first one (with a velocity $d\overline{\nu}/dP$ of 3.82 cm^{-1}/GPa with respect to 1.74 cm^{-1}/GPa, as reported in Table III). As a consequence, the separation between the two increases with pressure. By comparing our computed separation with the experimental one[23] (horizontal arrows in the figure), we can clearly see how accurately present calculations are describing the evolution under pressure of this feature of the spectrum. The small peak appearing at about 700 cm^{-1} (that could not be detected in the experiment by Kung *et al.*[23]) is the fastest one, evolving with a speed of 4.22 cm^{-1}/GPa whereas the slowest one is the peak at about 200 cm^{-1} with a speed of just 1.07 cm^{-1}/GPa. The Raman intensity decreases as a function of pressure for all peaks in the spectrum but #8 that shows an almost constant intensity on pressure, in agreement with experimental evidence. Intensities of different peaks vary differently with pressure. In particular, that of peak #7 decreases much more than that of peak #6, again in agreement with what reported by Kung *et al.*[23]

As a last point, we report the evolution under pressure of the computed IR spectrum of $CaSnO_3$. To the best of our knowledge, there are no experimental studies to compare with, in this respect. Given the fairly satisfactory description of the pressure dependence of the Raman spectrum discussed above, we consider these predictions to be rather reliable and to constitute a stimulating and useful starting point for further experimental measurements. In Figure 7, we report the computed IR spectrum at 8 different pressures from zero to 25 GPa. Selected peaks are labeled from #1 to #12 (both in the bottom and top spectra) to facilitate the discussion; the remaining 13 peaks have low intensity at zero pressure. From inspection of the figure we note that, as pressure increases, the spectrum becomes more structured; new peaks appear like #7, the one between #11 and #12 and that close to #4. All peaks are blue-shifted under increasing pressure even if with different speeds. Among the selected peaks, the slowest ones are #2 and #7 (with speeds of 1.59 and 1.77 cm^{-1}/GPa, respectively). The peaks with largest shift speed are #11 and #12 (4.70 cm^{-1}/GPa) and #8 (3.45 cm^{-1}/GPa). As regards the intensity, we note that it generally decreases with pressure but just by a relatively small amount (about 10 % for the highest peaks). An interesting feature of the spectrum is the inversion in relative intensity of peaks #8 and #9 at about 6 GPa.

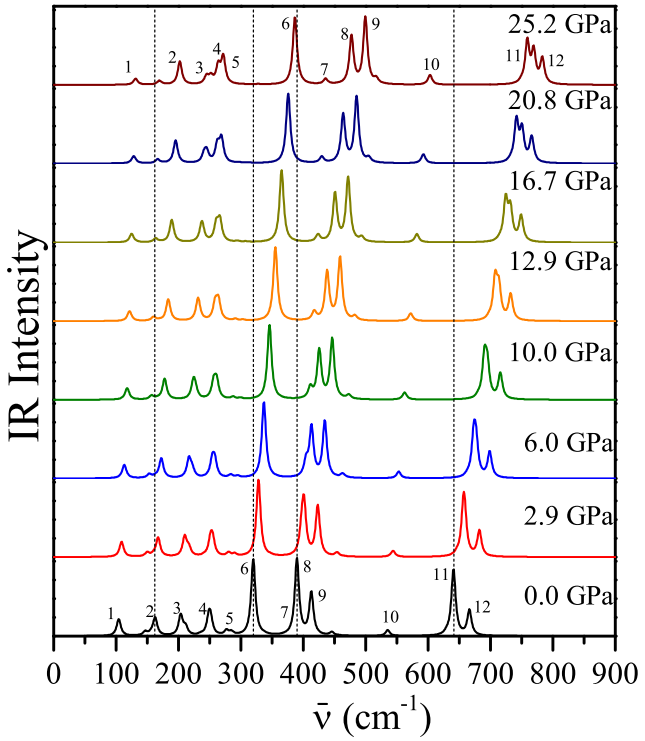

FIG. 7. (color online) Evolution under pressure, up to 25 GPa, of the computed IR spectrum of $CaSnO_3$. Intensities at all pressures are relative to the zero-pressure ones. Vertical dashed lines are just an eye-guide. In the zero pressure and 25 GPa spectra, selected peaks are labeled to facilitate the discussion in the text.

IV. CONCLUSIONS

The evolution under increasing pressure, up to 25 GPa, of the spectroscopic response of the calcium stannate, $CaSnO_3$, perovskite has been fully characterized by means of advanced *ab initio* simulations. The pressure dependence of phonon wave-numbers and infrared (IR) and Raman intensities is computed and compared with experimental data (when available). 25 IR and 24 Raman active peaks are computed, with respect to 5 and 12 experimentally reported ones. The theoretical description of the evolution under pressure of the Raman spectrum is found to closely match the experimental one. On these grounds, our predictions about the pressure dependence of the IR spectrum (which is not yet available experimentally) are expected to be reliable and to constitute a stimulus for further experimental measurements.

In order to achieve such a full characterization, the combined use of a large number of advanced algorithms (equation-of-state, elastic tensor calculation, phonon frequency evaluation, IR and Raman intensities via Coupled-Perturbed-Hartree-Fock/Kohn-Sham scheme), as recently implemented in the CRYSTAL14 program by some of the authors, was required. In particular, the analytical calculation of IR and Raman intensities for periodic systems has only recently become available and is here applied for the first time to investigate the pressure dependence of computed spectra. An accurate computational methodology, based on periodic *ab initio* simulations at B3LYP level of theory and using local Gaussian-type function basis set, has been devised for this purpose which has allowed to reliably discuss many structural, elastic and spectroscopic features of calcium stannate up to 25 GPa of pressure.

ACKNOWLEDGMENTS

J.M. acknowledges the Brazilian scholarship program "Ciência sem Fronteiras" (Process Number 248425/2013-7/SWE).

[1] A. M. Azad, L. L. W. Shyan, and M. A. Alim, J. Mater. Sci. **34**, 3375 (1999).
[2] A. M. Azad, L. L. Shyan, and M. A. Alim, J. Mater. Sci. **34**, 1175 (1999).
[3] H. Cheng and Z. Lu, Solid State Sciences **10**, 1042 (2008).
[4] N. Sharma, K. M. Shaju, G. V. Subba Rao, and B. V. R. Chowdari, Electrochem. Commun. **4**, 947 (2002).
[5] M. Mouyane, M. Womes, J. C. Jumas, J. Olivier-Fourcade, and P. E. Lippens, J. Solid State Chem. **184**, 2877 (2011).
[6] X. Hu, T. Xiao, W. Huang, W. Tao, B. Heng, X. Chen, and Y. Tang, Appl. Surf. Sci. **258**, 6177 (2012).
[7] W. Zhang, J. Tang, and J. Ye, J. Mater. Res. **22**, 1859 (2007).
[8] Z. Liu and Y. Liu, Mater. Chem. Phys. **93**, 129 (2005).
[9] B. Lei, B. Li, H. Zhang, and W. Li, Opt. Mater. **29**, 1491 (2007).
[10] B. Lei, B. Li, H. Zhang, L. Zhang, Y. Cong, and W. Li, J. Electrochem. Soc. **154**, H623 (2007).
[11] Z. Fu, W. Li, S. Du, H. K. Yang, and J. H. Jeong, J. Electrochem. Soc. **156**, J308 (2009).
[12] K. Ueda and Y. Shimizu, Thin Solid Films **518**, 3063 (2010).
[13] X. Y. Chen, C. Ma, S. P. Bao, and H. Y. Zhang, J. Alloys Compd. **497**, 354 (2010).
[14] X. L. Pang, C. H. Jia, G. Q. Li, and W. F. Zhang, Opt. Mater. **34**, 234 (2011).
[15] T. Nakamura, M. Shima, M. Yasukawa, and K. Ueda, J. Sol-Gel Sci. Technol. **61**, 362 (2012).
[16] Z. Liang, J. Zhang, J. Sun, X. Li, L. Cheng, H. Zhong, S. Fu, Y. Tian, and B. Chen, Physica B **412**, 36 (2013).
[17] A. M. Glazer, Acta Crystallogr., Sect. B: Struct. Sci **28**, 3384 (1972), 01787.
[18] P. M. Woodward, Acta Crystallogr., Sect. B: Struct. Sci **53**, 32 (1997), 00580.
[19] J. Kung, R. J. Angel, and N. L. Ross, Phys. Chem. Miner. **28**, 35 (2001).
[20] J. Zhao, N. L. Ross, and R. J. Angel, Phys. Chem. Miner. **31**, 299 (2004).
[21] T. Tsuchiya and J. Tsuchiya, Am. Mineral. **91**, 1879 (2006).
[22] G. R. Helffrich and B. J. Wood, Nature **412**, 501 (2001).
[23] J. Kung, Y. J. Lin, and C. M. Lin, J. Chem. Phys. **135**, 224507 (2011).
[24] B. W. Schneider, W. Liu, and B. Li, High Pressure Res. **28**, 397 (2008).
[25] S. Tateno, K. Hirose, N. Sata, and Y. Ohishi, Phys. Earth Planet. Inter. **181**, 54 (2010).
[26] M. C. F. Alves, S. C. Souza, H. H. S. Lima, M. R. Nascimento, M. R. S. Silva, J. W. M. Espinosa, S. J. G. Lima, E. Longo, P. S. Pizani, L. E. B. Soledade, et al., J. Alloys Compd. **476**, 507 (2009).
[27] L. Li, S. Peng, J. Wang, Y. L. Cheah, P. Teh, Y. Ko, C. Wong, and M. Srinivasan, ACS Appl. Mater. Interfaces **4**, 6005 (2012).
[28] M. C. F. Alves, R. M. M. Marinho, G. P. Casali, M. Siu-Li, S. Députier, M. Guilloux-Viry, A. Souza, E. Longo, I. T. Weber, I. M. G. Santos, et al., J. Solid State Chem. **199**, 34 (2013).
[29] P. McMillan and N. Ross, Phys. Chem. Miner. **16**, 21 (1988).
[30] M. Tarrida, H. Larguem, and M. Madon, Phys. Chem. Miner. **36**, 403 (2009).
[31] S. A. T. Redfern, C. Chen, J. Kung, O. Chaix-Pluchery, J. Kreisel, and E. K. H. Salje, J. Phys.: Condens. Matter **23**, 425401 (2011).
[32] E. V. Galuskin, I. O. Galuskina, V. M. Gazeev, P. Dzierzanowski, K. Prusik, N. N. Pertsev, A. E. Zadov, R. Bailau, and A. G. Gurbanov, Mineral. Mag. **75**, 2563 (2011).
[33] H. L. Zheng, Z. C. Zhang, J. G. Zhou, S. S. Yang, and J. Zhao, Appl. Phys. A **108**, 465 (2012).
[34] A. Yangthaisong, Chin. Phys. Lett. **30**, 077101 (2013).
[35] R. Dovesi, V. R. Saunders, C. Roetti, R. Orlando, C. M. Zicovich-Wilson, F. Pascale, K. Doll, N. M. Harrison, B. Civalleri, I. J. Bush, et al., *CRYSTAL14 User's Manual*, Università di Torino, Torino (2014), http://www.crystal.unito.it.
[36] R. Dovesi, R. Orlando, A. Erba, C. M. Zicovich-Wilson, B. Civalleri, S. Casassa, L. Maschio, M. Ferrabone, M. De La Pierre, Ph. D'Arco, et al., Int. J. Quantum Chem. **114**, 1287 (2014).
[37] L. Maschio, B. Kirtman, R. Orlando, and M. Rérat, J. Chem. Phys **137**, 204113 (pages 11) (2012).
[38] L. Maschio, B. Kirtman, M. Rérat, R. Orlando, and R. Dovesi, J. Chem. Phys **139**, 164102 (2013).
[39] A. D. Becke, J. Chem. Phys. **98**, 5648 (1993).
[40] A. Erba, K. E. El-Kelany, M. Ferrero, I. Baraille, and M. Rérat, Phys. Rev. B **88**, 035102 (2013).
[41] A. Mahmoud, A. Erba, K. E. El-Kelany, M. Rérat, and R. Orlando, Phys. Rev. B **89**, 045103 (2014).
[42] M. Prencipe, L. Maschio, B. Kirtman, S. Salustro, A. Erba, and R. Dovesi, J. Raman Spectrosc. **45**, 703 (2014).
[43] A. Erba, A. Mahmoud, D. Belmonte, and R. Dovesi, J. Chem. Phys. **140**, 124703 (2014).
[44] V. Lacivita, A. Erba, R. Dovesi, and Ph. D'Arco, Phys. Chem. Chem. Phys. **16**, 15331 (2014).
[45] A. Erba, A. Mahmoud, R. Orlando, and R. Dovesi, Phys. Chem. Miner. **41**, 151 (2014).

[46] A. Erba, A. M. Navarrete-López, V. Lacivita, P. D'Arco, and C. M. Zicovich-Wilson, Phys. Chem. Chem. Phys. (2015), dOI: 10.1039/C4CP04414B.
[47] M. Ferrero, M. Rérat, R. Orlando, and R. Dovesi, J. Comp. Chem. **29**, 1450 (2008).
[48] A. Erba, M. Ferrabone, R. Orlando, and R. Dovesi, J. Comput. Chem. **34**, 346 (2013).
[49] L. Valenzano, F. J. Torres, K. Doll, C. M. Zicovich-Wilson, and R. Dovesi, Z. Phys. Chem. **220**, 893 (2006).
[50] F. R. Sensato, L. Gracia, A. Beltrán, J. Andrés, and E. Longo, J. Phys. Chem. C **116**, 16127 (2012).
[51] J. Baima, A. Erba, M. Rérat, R. Orlando, and R. Dovesi, J. Phys. Chem. C **117**, 12864 (2013).
[52] K. Doll, Comput. Phys. Commun. **137**, 74 (2001).
[53] K. Doll, V. Saunders, and N. Harrison, Int. J. Quantum Chem. **82**, 1 (2001).
[54] C. G. Broyden, IMA J. Appl. Math. **6**, 76 (1970).
[55] R. Fletcher, Comput. J. **13**, 317 (1970).
[56] D. Goldfarb, Mathematics of Computation **24**, 23 (1970).
[57] D. F. Shanno, Mathematics of Computation **24**, 647 (1970).
[58] A. B. Alchagirov, J. P. Perdew, J. C. Boettger, R. C. Albers, and C. Fiolhais, Phys. Rev. B **63**, 224115 (2001).
[59] R. E. Cohen, O. Gülseren, and R. J. Hemley, Am. Mineral. **85**, 338 (2000).
[60] F. D. Murnaghan, Proc. Natl. Acad. Sci. USA **30**, 244 (1944).
[61] F. Birch, Phys. Rev. **71**, 809 (1947).
[62] F. Birch, J. Geophys. Res. **83**, 1257 (1978).
[63] J.-P. Poirier and A. Tarantola, Physics of the Earth and Planetary Interiors **109**, 1 (1998).
[64] P. Vinet, J. Ferrante, J. R. Smith, and J. H. Rose, J. Phys. C **19**, 467 (1986).
[65] A. Erba, M. Ferrabone, J. Baima, R. Orlando, M. Rérat, and R. Dovesi, J. Chem. Phys. **138**, 054906 (2013).
[66] J. F. Nye, *Physical properties of crystals* (Oxford University Press, Oxford, 1957).
[67] J. C. Tan, B. Civalleri, A. Erba, and E. Albanese, CrystEngComm **17**, 375 (2015).
[68] C. Carteret, M. De La Pierre, M. Dossot, F. Pascale, A. Erba, and R. Dovesi, J. Chem. Phys. **138**, 014201 (2013).
[69] M. Veithen, X. Gonze, and P. Ghosez, Phys. Rev. B **71**, 125107 (2005).
[70] D. Cherrad, D. Maouche, M. Boudissa, L. Reffas, M.and Louail, M. Maamache, K. Haddadi, and Y. Medkour, Physica B **429**, 95 (2013).
[71] A. Erba, J. Chem. Phys. **141**, 124115 (2014).
[72] R. Hill, J. Mech. Phys. Solids **11**, 357 (1963).
[73] G. Ottonello, B. Civalleri, J. Ganguly, W. F. Perger, D. Belmonte, and M. Vetuschi Zuccolini, Am. Mineral. **95**, 563 (2010).
[74] H. Mizoguchi, H. W. Eng, and P. M. Woodward, Inorg. Chem. **43**, 1667 (2004).
[75] J. M. Henriques, E. W. S. Caetano, V. N. Freire, J. A. P. da Costa, and E. L. Albuquerque, J. Phys.: Condens. Matter **19**, 106214 (2007).
[76] Graphical animations of all phonon modes can be viewed at http://www.crystal.unito.it/supplementary-materials.php.